J|A|C|S ARTICLES

Published on Web 04/20/2010

Reversible Twisting during Helical Hippuric Acid Crystal Growth

Alexander G. Shtukenberg,*,† John Freudenthal,‡ and Bart Kahr*,‡

Department of Chemistry, New York University, 100 Washington Square East, New York, New York 10003 and Crystallography Department, St. Petersburg State University, Universitetskaya emb., 7/9, 199034, St. Petersburg, Russia

Received February 27, 2010; E-mail: shtukenberg@mail.ru; bart.kahr@nyu.edu

Abstract: Crystals grow in the mind's eye by the addition of small units to a monolith each part of which is in fixed translational relation to every other part. Here, it is shown that growth can induce reversible twisting and *untwisting* of macroscopic crystals of hippuric acid (*N*-benzoylglycine, $C_9H_9NO_3$) on the scale of radians. Crystals growing in undercooled melts of hippuric acid twist about the axis of elongation. At the same time the twisting is undone by new elastic stresses that build up as the crystal thickens. The dynamic interplay of twisting and untwisting ultimately fixes the crystal morphology. A correspondence between the optical properties of hippuric acid single crystals and twisted needles measured with a Mueller matrix microscope is established. The measured crystalloptical properties are in complete accord with the optical indicatrix rotating helically along the axis of elongation at the growth front, or counter-rotating so as to unwind earlier growth. The reversible morphological changes captured here *in situ* are likely also found in banded spherulites of high molecular weight polymers, optically modulated chalcedony minerals, elements, proteins, and other molecular crystals for which there is evidence of helical twisting. The analysis of such systems is usually predicated on the relationship of crystalline helical pitch to a power law exponent. However, in the absence of previous considerations of untwisting, the mechanistic content of such relationships is questionable.

Introduction

Crystals with "noncrystallographic"[1] morphologies challenge our understanding of growth mechanisms and structures of organized matter. Triacontahedral quasicrystals[2] fall into this class, for example, as do crystals with mesoscale helical morphologies. The latter have been widely observed across the crystal kingdom, perhaps most dramatically in so-called biomorphs[3] that may inform our understanding of helical and spiral crystal forms of biological origin.[4] Moreover, self-assembling, helical nanofibers, the fruits of advances in all manner of microscopies, have been liberally sprinkled throughout the recent literature.[5]

Helically twisted crystals have been established unequivocally by microfocus X-ray diffraction,[6] small-angle X-ray scattering,[7] and selected area electron diffraction.[8] They have been observed growing *in situ* by atomic force microscopy.[9] Yet, despite progress in some areas, helical crystals are, *in the aggregate*, unfinished with respect to characterizations of structure and growth mechanism. For instance, large potassium dichromate helices were grown from gels, but they have not been indexed to the best of our knowledge.[10] Naturally occurring fibrous quartz (chalcedony) is undoubtedly helical in some occurrences, but the growth conditions cannot be reproduced in the laboratory.[11] Helical crystals are displayed abundantly in the high molecular weight polymer literature, but the mechanisms of crystal deformation have been subject to vigorous debate.[12] Further confounding is that some microscale helices, supposedly composed of barium carbonate, were devoid of inorganic matter; they were instead a consequence of the abrasion of polystyrene

† St. Petersburg State University.
‡ New York University.

(1) Cölfen, H.; Antonietti, M. *Mesocrystals and Nonclassical Crystallization*; John Wiley: Chesterfield, U.K., 2008.
(2) Dubost, B.; Lang, J.-M.; Tanaka, M.; Sainfort, P.; Audier, M. *Nature* **1986**, *324*, 48–50.
(3) Melero-García, E.; Santisteban-Bailón, R.; Garcia-Ruiz, J. M. *Cryst. Growth Des* **2009**, *9*, 4730–4734. García-Ruiz, J. M.; Melero-García, E.; Hyde, S. T. *Science* **2009**, *323*, 362–365. Bittarello, E.; Aquilano, D. *Eur. J. Mineral* **2007**, *19*, 345–351.
(4) Hildebrand, M.; Doktycz, M. J.; Allison, D. P. *Pflugers Arch. - Eur. J. Physiol.* **2008**, *456*, 127–137.
(5) Green, M. M., Nolte, R. J. M., Meijer, E. W., Eds. *Materials—Chirality*; Denmark, S. E., Siegel, J., Series Eds.; Topics in Stereochemistry; John Wiley: Hoboken, NJ, 2003 Vol. 24. Amabilino, D. B., Ed. *Chirality at the Nanoscale*; Wiley-VCH: Weinheim, 2009. Shimizu, T.; Masuda, M.; Minamikawa, H. *Chem. Rev* **2005**, *105*, 1401–1443. Brizard, A.; Oda, R.; Huc, I. *Top. Curr. Chem.* **2005**, *256*, 167–218.
(6) Gazzano, M.; Focarete, M. L.; Riekel, C.; Scandola, M. *Biomacromolecules* **2004**, *5*, 553–558.
(7) Wang, X.; Lu, Y.; Duan, Y.; Meng, L.; Li, C. *Adv. Mater.* **2008**, *20*, 462–465.
(8) Jin, S.; Jeong, K. U.; Tu, Y.; Graham, M. J.; Wang, J.; Harris, F. W.; Cheng, S. Z. D. *Macromolecules* **2007**, *40*, 5450–5459.
(9) Xu, J.; Guo, B.-H.; Zhang, Z.-M.; Zhou, J.-J.; Jiang, Y.; Yan, S.; Li, L.; Wu, Q.; Chen, G.-Q.; Schultz, J. M. *Macromolecules* **2004**, *37*, 4118–4123.
(10) Suda, J.-I.; Matsushida, M. *J. Phys. Soc. Jpn.* **2004**, *73*, 300–302.
(11) Frondel, C. *Am. Mineral.* **1978**, *63*, 17–27.
(12) (a) Lotz, B.; Cheng, S. Z. D. *Polymer* **2005**, *46*, 577–610. (b) Bassett, D. C. *Polymer* **2006**, *47*, 3263–3266. (c) Lotz, B.; Cheng, S. Z. D. *Polymer* **2006**, *47*, 3267–3270.

containers.[13] Helical ribbons of molecular crystals such as decacyclene[14] or 10,12-tricosadynoic anhydride[15] can be easily grown from solution, but the optical analyses of helical precession are complicated by the presentation of steep angles of incidence and extreme fragility. We set out to establish conditions for the *in situ* optical analysis of a simple, helical crystal. We chose hippuric acid (HA, or *N*-benzoylglycine, $C_9H_9NO_3$) as a model because helical polycrystalline, spherulitic ensembles were described by Gaubert,[16] Bernauer,[17] and Hartshorne.[18] Individual helical HA crystals were described by Calvert and Uhlmann.[19,20]

Here, we establish that HA crystal twisting is not fixed during growth. It is reversible, wholly or in part. This observation calls to question a large body of literature that has attempted to use the helix period, *P*, to establish growth mechanisms. Moreover, our observations place constraints on previously proposed mechanisms for crystal twisting.

Crystal Characterization Including Experimental

The only identified phase of HA belongs to the orthorhombic system, space group $P2_12_12_1$, with lattice constants $a = 9.112(2)$ Å, $b = 10.566(2)$ Å, $c = 8.855(2)$ Å.[21] Single crystals grown by evaporation of acetone exhibit primarily {001}, {011}, {100}, {101}, {110} facets.[22] The refractive indices are $n_X = 1.535$, $n_Y = 1.592$, $n_Z = 1.760$ (optic plane is (100), $2V(+) = 66°$).[22] Very strong linear birefringence $n_Z - n_X = 0.225$ and $n_Z - n_Y = 0.168$ can be accounted for by the strong polarizability expected along the [010] direction, which is nearly parallel to the phenyl rings and perpendicular to the page in Figure 1. Thus, the orientation of the optical indicatrix (refractive index ellipsoid) is *X*||[001], *Y*||[100], and *Z*||[010]. Figure 1 also shows the orientation of the optic axes (OAs) in stereographic projection with respect to the crystal structure viewed along the *b* axis.

The optical properties were established with a home-built Mueller matrix microscope (MMM)[23] constructed from a 532 nm Nd:YAG laser (Lasermate), a fiber optic phase scrambler, two linear polarizers, two achromatic quarter wave plates, two achromatic half wave plates mounted in rotation stages (Thorlabs), and a QSI 532 CCD camera. Glass slides were mounted on Thorlabs rotation stages. Mueller matrices were inverted[24] from 36 intensity images at wave plate positions chosen near optimal inversion conditions.[25]

A small amount (1−5 mg) of HA (98% Sigma-Aldrich) was placed between a microscopic slide and cover glass. Experiments were likewise carried out with HA once recrystallized from ethanol. HA was melted on a hot plate, after which the sample was immediately quenched in air at room temperature. A thin film of the melt (typically 5−8 μm) crystallized during rapid cooling. The sample was remelted with a hot stage (Model FP90, Mettler-Toledo) up to 188.3−190 °C (melting point $T_{melt} = 188$ °C) and cooled at a rate of 20 °C/min to the desired crystallization temperature.

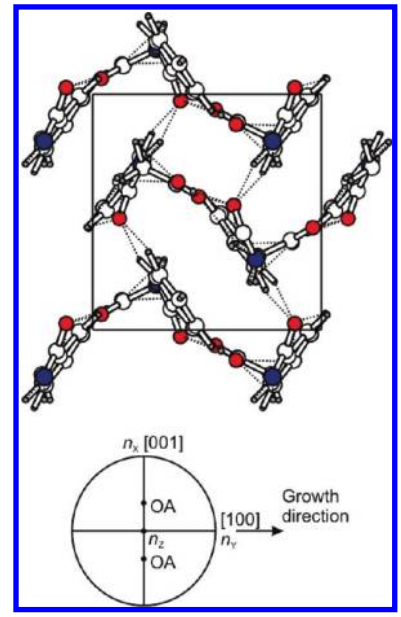

Figure 1. Crystal structure of HA projected onto (010) plane. Red atoms = oxygen; blue = nitrogen; gray = hydrogen; colorless = carbon. The corresponding stereographic projection of the optical indicatrix with optic axis (OA) outcrops is displayed.

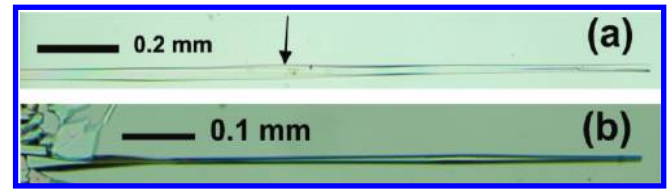

Figure 2. Morphological evidence of HA needle twisting. (a) Twisting edge (see arrow) dividing two growth sectors (presumably {011}) crossing the needle in the middle ($\Delta T = 23$ °C). (b) Change of the crystal width along the needle indicates growth rate anisotropy normal to the growth direction in the (100) plane ($\Delta T = 12$ °C).

At comparatively low supercooling of the melt ($\Delta T < 15$ °C) [100] needles form, bounded by {011}, {100}, and {101} faces; they are not twisted or branched. At higher supercooling ($\Delta T = 15-28$ °C) the crystals start to twist.

The twisting of needles formed under these conditions is evident by inspection. In Figure 2a one can see the line separating two facets running diagonally along the crystal length at the center ($\Delta T = 23$ °C). In Figure 2b, the periodic change of width indicates growth rate anisotropy normal to the growth direction in the (100) plane ($\Delta T = 12$ °C).

Crystallization was observed *in situ* and documented with a polarized light microscope (Olympus BX-50) equipped with a digital camera (Nikon D-80). An assortment of needles pictured in Figure 3 grew at $\Delta T > 15$ °C at rates of 20−100 μm/s. HA needles in general orientations are bright between crossed linear polarizers, but they are punctuated by dark bands, the outcrops of the OAs of the biaxial HA crystals. In longer needles, not captured in a single frame, the position of OA outcrops can be marked with respect to the growing tip (Figure 4). The

(13) Glabb, F.; Kellermeier, M.; Kunz, W. *Macromol. Rapid Commun.* **2007**, *28*, 1024–1028.
(14) Ho, D. M.; Pascal, R. A., Jr. *Chem. Mater.* **1993**, *5*, 1358–1361.
(15) Lindsell, W. E.; Preston, P. N.; Seddon, J. M.; Rosair, G. M.; Woodman, T. A. *J. Chem. Mater.* **2000**, *12*, 1572–1576.
(16) Gaubert, P. *C. R. Acad. Sci. (Paris)* **1927**, *184*, 1565.
(17) Bernauer, F. *"Gedrillte" Kristalle*; Gebrüder Borntrager: Berlin, 1929.
(18) Hartshorne, N. H. *Nature* **1961**, *190*, 1191.
(19) Calvert, P. D.; Uhlmann, D. R. *J. Polym. Sci., Polym. Phys. Ed.* **1973**, *11*, 457–465.
(20) These structures have also been observed by A. Lovinger, private communication.
(21) Nagaraja, H. S.; Upahyaya, V.; Rao, P. M.; Aithal, P. S.; Bhat, A. P. *J. Cryst. Growth* **1998**, *193*, 674–678.
(22) Winchell, A. N. *The Optical Properties of Organic Compounds*; McCrone Research Institute: Chicago, 1987; p 113.
(23) Goldstein, D. *Polarized Light*; Marcel Dekker: New York, 2003.
(24) Chipman, R. A. In *Handbook of Optics, Vol. II*; Bass, M., Ed.; McGraw-Hill: 1995; Chapter 22.
(25) Smith, M. H. *Appl. Opt.* **2002**, *41*, 2488–2493.

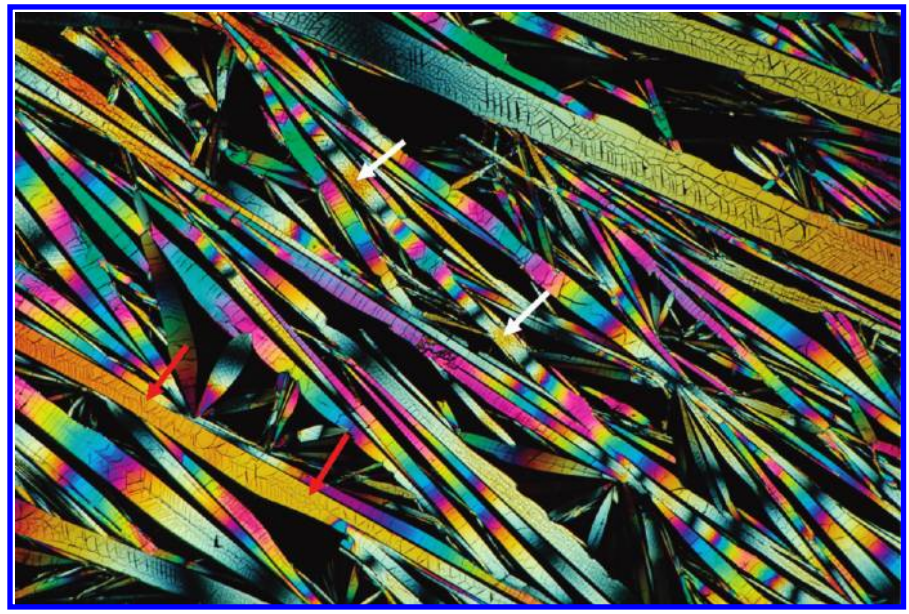

Figure 3. Assortment of HA needles grown from the melt viewed between crossed polarizers in white light. White arrows mark a highly twisted crystal with a succession of OA outcrops. Most needles are crystallographically twisted as indicated by the modulation of the interference colors. However, the large crystal running from top left to lower right, indicated by red arrows, has largely completed the process of untwisting evidenced by the homogeneous retardance. See Figure 9. While the ribbon marked by the white arrows is crystallographically helical, it paradoxically appears to be flat, constrained by the plane parallel glasses of its container. Horizontal dimension of photograph is 2.2 mm.

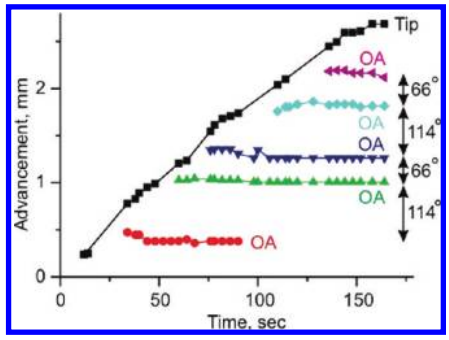

Figure 4. Growth evolution of a HA needle. The distance between crystal Tip, outcrops of optic axes (OAs), and the needle origin as a function of growth time. Long and short spacing between OAs alternate due to the anisotropy of the optical indicatrix. Linear distances are roughly proportional to angular distances between OA outcrops (66° and 114°). The position of the red OA was terminated as it was no longer in the field of view, focused on the tip.

appearance of successive OA outcrops is interpreted as a rotation of the optical indicatrix via growth induced twisting (a movie of twisting/untwisting is available in the Supporting Information). Twisted HA crystals have been described previously.[16−19]

Crystal length and width were measured directly from images, and the thickness was determined from retardation at points with maximum (minimum) birefringence (assuming theoretical values based on previously determined refractive indices).[22] The twist period was determined from the band spacing or distance between the outcrops of OAs.

Figure 4 represents the optical evolution of a single, as-grown crystal. A full twist (2π) of the HA needles consists of two equivalent half periods that each expose outcrops of the two OAs, so long as the optic plane is perpendicular to the fiber extension (see Figure 1). Such OAs would not be spaced evenly along the needle because the splitting or biaxial angle ($2V$) is not 90°; rather it is 66°. Thus, each half period is divided into a long and a short spacing between OA outcrops corresponding to angular rotations of 66° and $\pi - 66° = 114°$. This spacing is manifest in five OAs tracked in Figure 4.

The linear anisotropies of the sample were accurately measured with a Mueller matrix microscope (MMM). A MMM analyzes the polarization properties of a sample in terms of the transformation of an input Stokes vector (S_{in}, eq 1) via the Mueller matrix (M): $S_{out} = MS_{in}$.[26] Here, E_x and E_y are orthogonal electric field components.

$$S = \begin{bmatrix} |E_x|^2 + |E_y|^2 \\ |E_x|^2 - |E_y|^2 \\ 2\mathscr{R}(E_x E_Y^*) \\ 2\mathscr{I}(E_x E_Y^*) \end{bmatrix} \tag{1}$$

$$I = \begin{bmatrix} S_{out}^T(\theta_1') \\ S_{out}^T(\theta_2') \\ S_{out}^T(\theta_3') \\ \vdots \\ S_{out}^T(\theta_n') \end{bmatrix} M[S_{in}(\theta_1) \quad S_{in}(\theta_2) \quad S_{in}(\theta_3) \quad \cdots \quad S_{in}(\theta_n)] \tag{2}$$

$\mathscr{R}$ is the real part, and $\mathscr{I}$ is the imaginary part. S_{out} is the output Stokes vector. An MMM is a crossed polarizer microscope with two rotating quarter wave plates added above and below the sample that act as a complete PSG/PSA pair. By collecting images as a function of rotations of the PSA (θ) and PSG (θ'), eq 2 can be applied to the recorded intensities (I) to solve the M of a sample at each pixel through pseudoinversion.[27] A MMM generates 16 images, each representing one of the elements of the 4 × 4 Mueller matrix expressed in terms of measurable input and output polarization state intensities. Our instrument is based on designs found elsewhere.[28−30]

(26) Azzam, R. M. A.; Bashara, N. M. *Ellipsometry and Polarized Light*, North Holland, Amsterdam, 1977.
(27) Takakura, Y.; Ahmad, J. E. *Opt. Soc. Am.* **2007**, *46*, 7354–7364.

Unfortunately, the 16 images are not simply related to the fundamental optical constants of interest: absorbance (A), linear birefringence (LB), linear birefringence with axes at 45° with respect to those of LB (LB'), linear dichroism (LD), linear dichroism with an axis at 45° with respect to those of LD (LD'), circular birefringence (CB), and circular dichroism (CD).[31] While this is standard nomenclature, we must be careful to avoid confusion. For instance, LB is the *retardance* ($2\pi(n_x - n_y)L/\lambda$ where L is the thickness and λ is the wavelength) related to linear birefringence ($n_x - n_y$) as ordinarily defined. $LB' = 2\pi(n_{45°} - n_{-45°})L/\lambda$. $CB = 2\pi(n_L - n_R)L/\lambda$, where n_L/n_R are refractive indices for left/right circularly polarized light. The contributions of the fundamental optical quantities to each matrix element were first derived by Jensen et al.,[32] and the full set of definitions are given in Table 2, ref 31.

To achieve the separation of optical effects, we have implemented the differential analysis pioneered by Azzam (eq 3):[26,33]

$$S(z + \Delta z) = M_{z,\Delta z}S(z), \text{ where } dS/dz = mS,$$
$$m = \lim_{\Delta z \to 0} \frac{M_{z,\Delta z} - I}{\Delta z}, \text{ and} \quad (3)$$

$$m = \begin{bmatrix} A & LD & LD' & CD \\ LD & A & CB & LB' \\ LD' & -CB & A & LB \\ CD & -LB' & -LB & A \end{bmatrix} \quad (4)$$

Here, z is the distance of propagation and m (eq 4) is the differential Mueller matrix describing the transformation of the Stokes vector for some infinitesimally small path Δz. The differential eq 3 can be integrated to give eq 5:

$$S_{out} = e^{mz}S_{in} = MS_{in} \quad (5)$$

The matrix m can be obtained numerically.[34] The process of deriving the differential matrix m unfolds the convolution of first-order optical properties[35] so that each fundamental quantity has a unique place in the matrix as in eq 4. This decomposition[36] of the resulting Mueller matrices (M) in Figure 3 subverts ambiguities[37] resulting from decomposition methods that parse M into noncommuting components.[38,39]

The total retardance of the system is taken as $\delta = (LB^2 + LB'^2 + CB^2)^{1/2}$. Polarization modulation methods return only asin(sin δ) which is $|\delta|$. After $|\delta|$ rises past π, it begins to decrease until it reaches 0. Then it rises again. This cycling can be seen in images (Figure 5a) and plots (Figure 5b) of $|\delta|$ as a function of needle extension. One can see that the order of the retardance is not measurable from the Mueller matrix at a single position. The so-called "order problem" was previously solved for a given position using multiple wavelengths.[40] For HA needles, we know that δ will vary smoothly as the crystal twists about an axis perpendicular to the wave vector. To measure the sample's total δ, $|\delta|$ needs to be unfolded as a function of needle position to resolve the ambiguity of the order. The unfolding procedure is analogous to phase unfolding or unwrapping in interferometry.[41] In brief, the first derivative of the function in Figure 5b was computed. At places near 0 and π where the first derivative was zero, the "up-needle", data to the right in Figure 5b, were reversed in the sign of the ordinate and that portion of the inverted function was translated so as to maintain continuity of the fuction. The procedure was continued iteratively for the remaining "up-needle" data. The unfolded

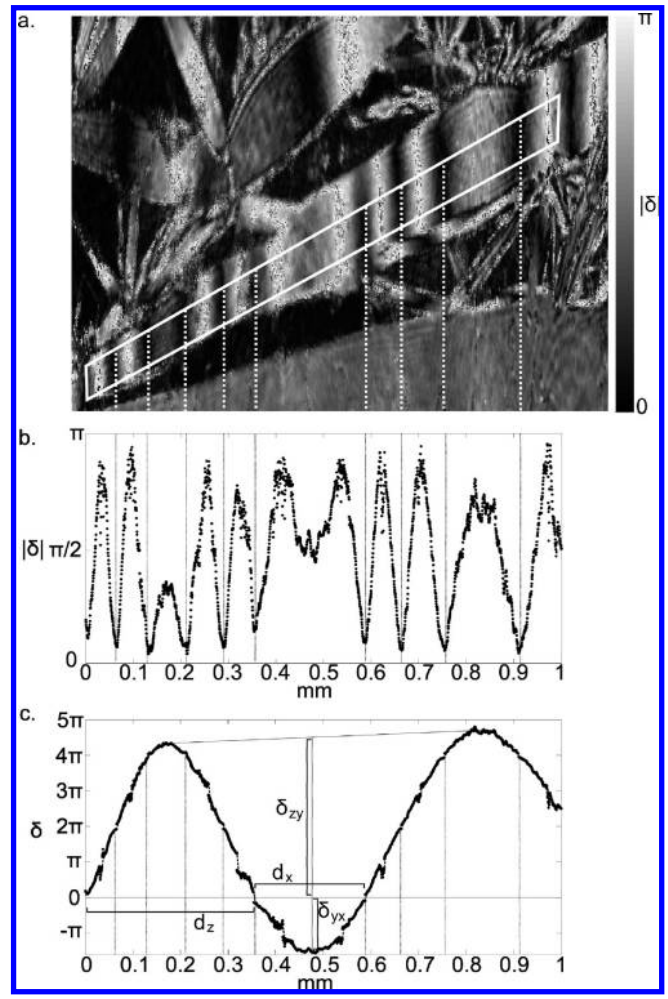

Figure 5. (a) A plot of the absolute value of the total retardance, $|\delta|$, at 532 nm. This quantity is obtained from the experimental Mueller matrices that contain a sin δ dependence. Dark bands indicate changes in phase by $2\pi m$ (where m = 0, 1, 2...) while dotted guidelines establish a correspondence between them and the data in (b) and (c). The thick needle located in the bottom of (c) presumably untwisted as the birefringence is not modulated. (b) The values of $|\delta|$ taken from the pixels within the white parallelogram in (a). This function thus contains an ambiguity regarding the order of the total δ. Only $|\delta|$ is derived from asin(sin δ). (c) δ is derived from $|\delta|$ by an unfolding process described in the text.

(28) Azzam, R. M. A. *Opt. Lett.* **1978**, *2*, 148–150.
(29) Goldstein, D. H. *Appl. Opt.* **1992**, *31*, 6676–6683.
(30) Hauge, P. S. *J. Opt. Soc. Am.* **1978**, *68*, 1519–1528.
(31) Schellman, J.; Jensen, H. P. *Chem. Rev.* **1987**, *87*, 1359–1399.
(32) Jensen, H. P.; Schellman, J. A.; Troxell, T. *Appl. Spectrosc.* **1978**, *32*, 192–200.
(33) Azzam, R. M. A. *J. Opt. Soc. Am.* **1978**, *68*, 1756–1767.
(34) Cheng, S. H.; Higham, N. J.; Kenney, C. S.; Laub, A. J. *SIAM J. Matrix. Anal. Appl.* **2001**, *22*, 1112–1125.
(35) Schellman, J.; Jensen, H. P. *Chem. Rev.* **1987**, *87*, 1359–1399.
(36) Azzam, R. M. A.; Bashara, N. M. *J. Opt. Soc. Am.* **1972**, *62*, 1252–1257. Mosino, J. F.; Starodumov, A.; Barbosa-Garcia, O.; Filippov, V. N. *J. Opt. B: Quantum Semiclassical Opt.* **2001**, *3*, S159.
(37) Savenkov, S. N.; Sydoruk, O. I.; Muttiah, R. S. *Appl. Opt.* **2007**, *46*, 6700–6709.
(38) Lu, S. Y.; Chipman, R. A. *J. Opt. Soc. Am. A* **1996**, *13*, 1106–1113.
(39) Savenkov, S. N.; Oberemok, Y. A. *Coherent Optics of Ordered and Random Media IV. SPIE* **2004**, *5475*, 99–107.
(40) Geday, M. A.; Kaminsky, W.; Lewis, J. G.; Glazer, A. M. *J. Microsc.* **2000**, *198*, 1–9.
(41) Pritt, M. D.; Ghiglia, D. C. *Two Dimensional Phase Unwrapping: Theory, Algorithms, and Software*; Wiley Interscience: 1998.

data in Figure 5c trace a smooth sinusoid along its length as the crystal rotates.

The spacings d_x and d_z in Figure 5b are in a ratio of 1.53. This compares with 114°/66° = 1.73, determined by the biaxial angle. This modest agreement between theory and experiment is easily explained when we address the untwisting that is a characteristic of HA needles (see next section). Because the thickness of the needles is not known precisely, we can only compare the values of retardance in Figure 5c as a ratio: $\delta_{xz}/\delta_{yx} = 2.89$ which should be equal to $(n_Z - n_Y)/(n_Y - n_X) = 0.168/0.057 = 2.95$. This better agreement between theory and experiment is expected here because no matter the pitch, the crystals must pass through the acute and obtuse bisectrices, those directions between OAs where Δn is a local maximum.

Twisting in [100] needles was confirmed by tilting a crystal around its elongated axis. Upon tilting, interference colors and OA outcrops were shifted along the fiber. This procedure, known as "sensing the screw", has established crystal helicity in a variety of materials.[17,18,42] Figure 6a shows the variable position of the extinction bands as a function of tilt angle (ϕ) about the needle axis. Figure 6b plots the variation of δ for the data contained in white boxes in Figure 6a. Figure 6c shows the continuous variation of δ as a function of position with tilt axis.

In a given melt, there was an equal population of left and right handed screws, presumably corresponding to enantiomorphous $P2_12_12_1$ crystals. However, it would be an understatement to describe the assignment of the absolute structure of such small crystals embedded within the melt as "difficult": we have not been able to obtain optical or morphological evidence of the structure sense, and the anomalous dispersion manifest in Friedel pairs of the C,H,N,O containing compound would be very small, even if we could isolate a single needle from the melt.

The data in Figure 4 are from a crystal that twisted as it grew and remained in the twisted state. As each OA turned in succession at the tip to become parallel to the wave vector of the transmitted light, the dark band between crossed polarizers that marked its position remained fixed along the length. This crystal, while illustrative of the shape of the optical indicatrix, was not typical of a given population of crystals that formed in a given undercooled glass.

Twisting Dynamics

Twisting dynamics depends on needle thickness. A sequence of images of the development of a very thin (<1.5 μm at the beginning of observation) HA needle is presented in Figure 7a taken between 2 and 24 s after the crystal was first detected. A movie showing the growth of this needle is provided as Supporting Information. At 2 s there is one "OA" labeled yellow and another "OA" labeled red. As the needle grows to the right, the yellow OA *moves* toward the growing tip (5 s). As the crystal thickens far from the tip, the induced twist unwinds. However, the red OA then disappears at 5 s (Figure 7b). In other words, the period (P) and associated twist angle $\theta = 2\pi/P$ arising on the crystal tip does not necessarily remain constant during subsequent growth. This occurs when the needle thickness is less than the spacing (Figure 7c) between glasses, when the crystal is fully surrounded by melt. During the first 12 s of observation the distance between OA outcrops, corresponding

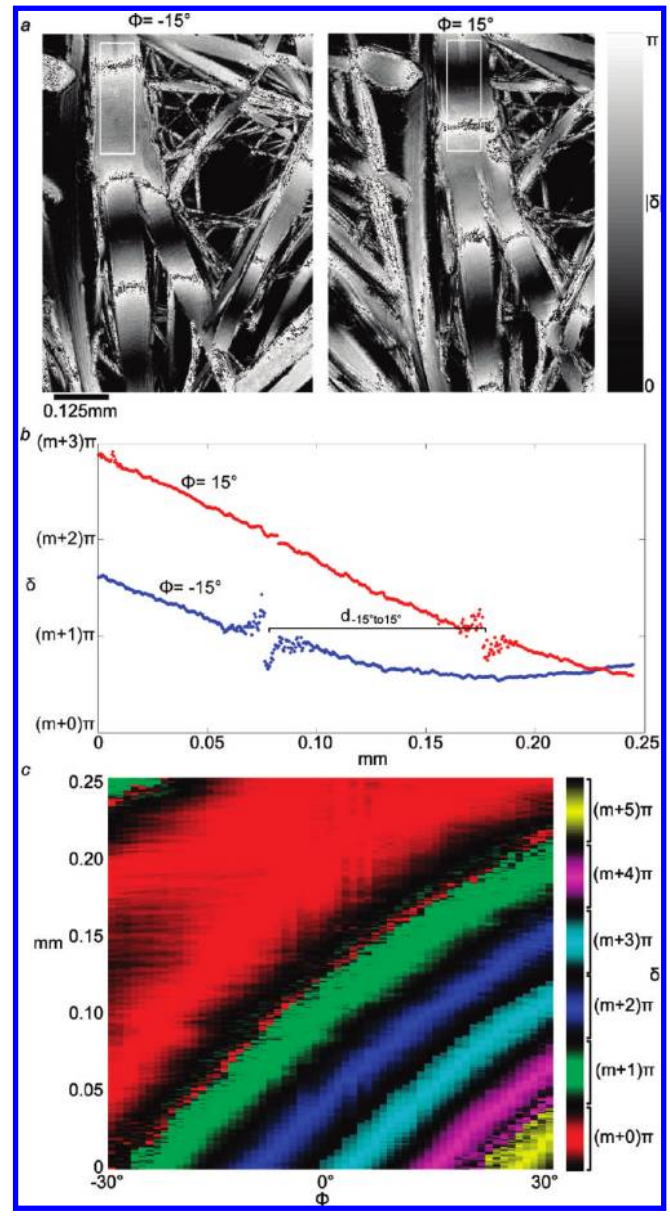

Figure 6. Sensing the screw. (a) |δ| image, at 532 nm, of HA needle twisted counterclockwise and clockwise by $\phi = \pm 15°$ about the vertical axis. Dark band (OA outcrop) has moved up and down within the white rectangle. (b) Plot of the numerical data contained within the white rectangles in (a). (c) Plot of positions of the OA outcrops as a function of tilt (ϕ) and extension along the needle.

to an angular rotation of 66°, increases linearly with the cylindrical crystal radius r; the twist period $P = 2\pi/\theta \propto r$. This linearity is also evident for other needles measured (Figure 8) implying that the crystal is *untwisting* as it is getting thicker. Since the needle cross section is elliptical, the effective radius r has been calculated from the measured width w and thickness h assuming a fixed torsion constant $J = \pi r^4/2 = \pi w^3 h^3/16(w^2 + h^2)$.[43]

Twisting is clearly correlated with the morphology of the tip. The tip can be rectilinear (Figure 9a) or increasingly lance-like (Figure 9b, c). Sharp tips twist more effectively. The tip sharpens when the melt is held for longer times near the melting temperature. Under these conditions, HA begins to slowly

(42) (a) Ye, H.-M.; Xu, J.; Guo, B.-H.; Iwata, T. *Macromolecules* **2009**, *42*, 694–701. (b) Maillard, D.; Prud'homme, R. E. *Macromolecules* **2008**, *41*, 1705–1712. (c) Keith, H. D.; Padden, F. J. *J. Polym. Sci.* **1959**, *39*, 101–122. (d) Keith, H. D.; Padden, F. J. *J. Polym. Sci.* **1959**, *39*, 123–138.

(43) Timoshenko, S.; Goodier, J. N. *Theory of Elasticity*; McGraw Hill: Singapore, 1982.

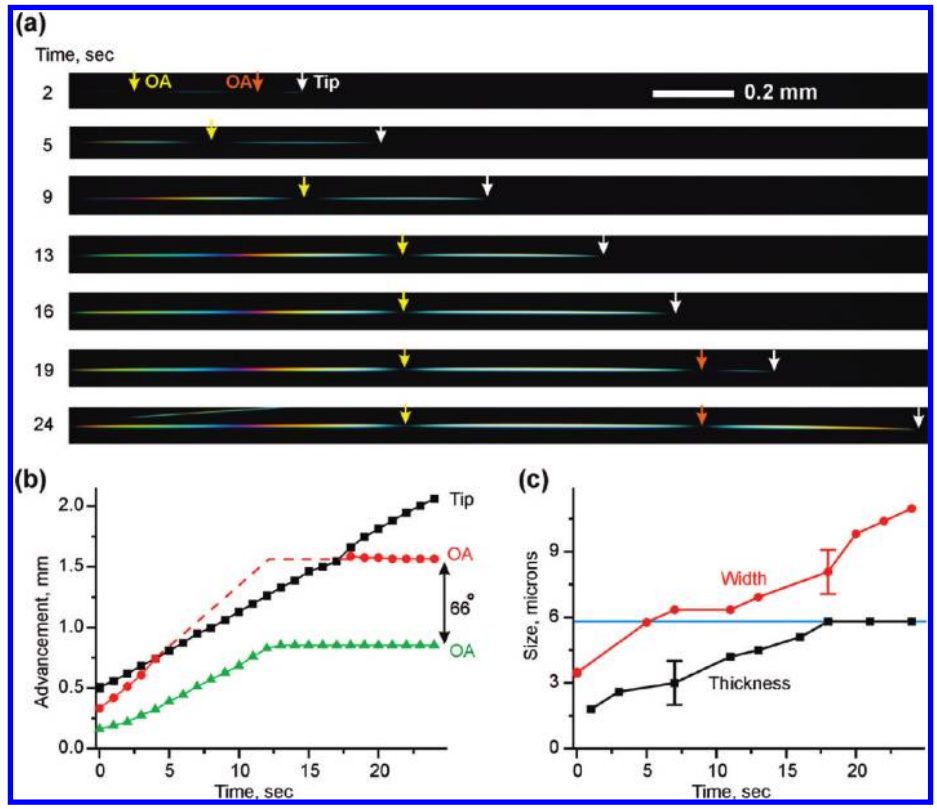

Figure 7. (a) Evolution of a HA needle in sequence of images between crossed polarizers. "OA" marks those spots where an OA is normal to the slide surface. (b) The advancement of a HA tip and two OAs as a function of growth time. Note that the red OA "disappears" (is pushed past the tip due to untwisting). (c) Averaged needle width and thickness as a function of growth time. Horizontal line shows thickness of the melt layer between glasses.

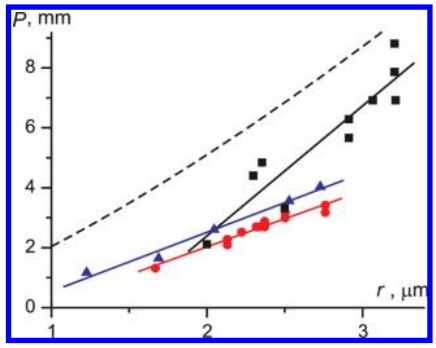

Figure 8. Increasing twist period for three HA needles represented as circles (red), triangles (blue), and squares (black) during thickening. The dashed line is Calvert and Uhlmann's[19] fit to their experimental data for individual HA crystals.

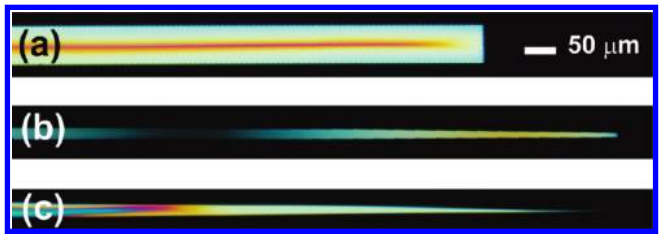

Figure 9. Evolution of the tip shape of HA needle-like crystals with increasing concentration of red decomposition product. White light between crossed polarizers. (a) Growth at $T = 178$ °C, held near melt temperature for $t \approx 5$ min; (b) $T = 173$ °C, $t \approx 15$ min; (c) $T = 175$ °C, $t \approx 21$ min.

decompose, evidenced by the fact that the melt takes on a bright-red color. The impurities were not detectable by NMR but presumably affect the growth.

Shortly after 12 s, the crystal in Figure 7 becomes as thick as the spacing between glasses and the untwisting ceases because of mechanical constraints. At the same time, crystal growth continues at the tip of the now thicker needle but the twist imparted here is no longer subject to change. Thus, the final twist period is the result of a two-stage process: (1) twisting, which occurs at the tip (the actively twisting tip is on the order of 10 μm or less) of the growing HA crystal; and (2) untwisting, associated with a whole crystal, so long as its surface is surrounded by the melt and it is not obstructed by the container. Local obstacles (e.g., other crystals) can also impede untwisting leading to a dispersion of periods within a given ensemble of crystals (see Figures 3 and 5a). Helical crystals with variable pitch were described previously.[44]

In the course of untwisting, the thicker, immobile part of the crystal forces the remainder to untwist completely. As a result, all traces of twisting in a once helical crystal may have vanished (Figure 10). Analogously, Shaskol'skaya and Pashkov bent a single crystalline rock-salt plate plastically. After submerging the deformed crystal into a supersaturated salt solution, the plastic deformation was undone by subsequent growth.[45] Bechhoefer and Hutter observed "unbanding" of spherulites of 4-cyano-4′-decyloxybiphenyl. This transformation does not appear to be untwisting as described here, but rather a phase change to another polymorphic form following nucleation and growth.[46]

(44) Li, C. Y.; Ge, J. J.; Bai, F.; Calhoun, B. H.; Harris, F. W.; Cheng, S. Z. D.; Chien, L.-C.; Lotz, B.; Keith, H. D. *Macromolecules* **2001**, *34*, 3634–3641.
(45) Shaskol'skaya, M. P.; Pashkov, P. P. *Sov. Phys. Crystallogr.* **1961**, *6*, 381.
(46) Hutter, J. L.; Bechhoefer, J. *J. Cryst. Growth* **2000**, *217*, 332–343.

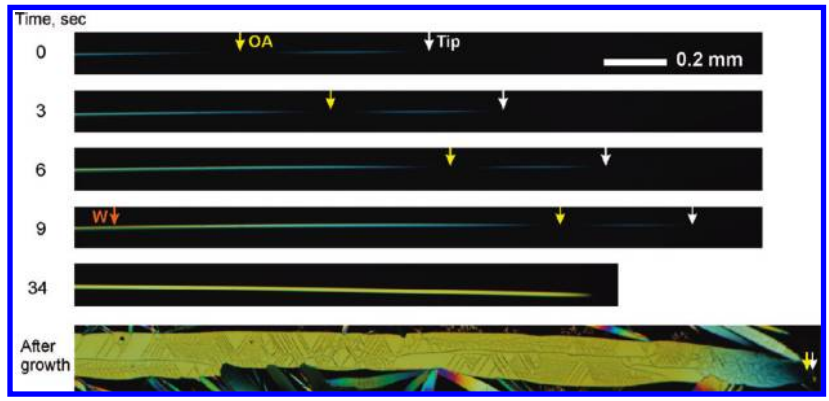

Figure 10. Evolution of HA needle growing to the right. OA marks outcrops of an optic axis; W marks point where the crystal thickness is becoming equal to the glass spacing. As 34 s, the left-most part of the crystal begins to thicken and the interference color along the entire length becomes uniform, indicating that the untwisting is complete for the section shown.

Another needle (Figure 4) did not show any change of twist period during growth despite its comparatively small width and thickness. In this case the needle was most likely adhered to one of the glasses impeding reorientation. However, 100 s later, the crystal broke loose initiating the anticipated untwisting for the thin needle. Collisions with other growing needles work likewise: they physically fix some section of the crystal, prevent its rotation around the needle axis, and freeze the existing pitch.

Twisting at the tip of growing HA crystals is a plastic deformation that requires that the operative stress exceed the critical shear stress τ_{crit}. We approximate a needle as a cylinder with the radius r, twist angle $\theta = 2\pi/P$, where observed HA helix parameters are $\theta = 1.6$ mm^{-1} and $r = 2.5$ μm. From these values we calculate a maximal shear stress, $\tau_{max} = \theta rG \approx 10^{-2}G$, where G is the shear modulus, a very large value ($\tau_{crit} = 10^{-5}G$ for ductile metals and $10^{-3}G$ for brittle salts at room temperature).[47] As the temperature rises to the melting point, the critical shear stress decreases exponentially. Although we do not know the value of τ_{crit} for HA, at growth temperatures where $T/T_{melt} = 0.93-0.97$, this value must be much lower than the applied stress (τ_{max}). Thus, elastic stress at the crystal tip must relax quickly by dislocation formation. The ensemble of dislocations is responsible for the observed twist deformation.

Thickening of the needle subsequent to twisting leads to a compensatory stress as forces draw the crystal into an arrangement with long-range translational order. The release of the plastic deformation is achieved by redistributing dislocations and increasing the twist period. Untwisting proceeds as described previously until the crystal is confined by its container or is otherwise mechanically constrained, after which the twist at that moment is preserved.

Twisting followed by untwisting complicates using $P(r)$ relationships for understanding the deformation mechanism. Usually we do not know the size of the crystal tip and, correspondingly, how the crystal thickness increases during growth. According to our data, during untwisting P is linearly proportional to r. This relationship could not be simpler. However, if we adopt an alternative description of the power law, commonly invoked in the literature, then we would surmise that P is proportional to r^n, where $n = 1$. If we maintain this description throughout crystal growth, then the exponent becomes greater than 1 during untwisting. Table 1 describes power laws previously derived for helical crystals, both helices in close packed spherulites and individual needles. Exponents vary from 0.3 for oxalic acid needles and reach 14.2 for poly(3-hydroxylbutyrate). What does this mean? Isolated needles should be more strongly twisted than tightly packed spherulite fibers, as indicated by the smaller exponents (Table 1). Other than that, data in the aggregate are likely compromised in part by untwisting and are of little mechanistic value.

Table 1. Power Law Relationship between Twist Period P, Cylindrical Fiber Radius r, and Supercooling ΔT; the Relationship $r \approx 1/\Delta T$ Is Usually Assumed[69] [a]

Substance	Power law	Reference
Spherulites		
Poly(hydroxybutyrate)	$P \propto (\Delta T)^{-4.9}$ [b]	48
Poly(3-hydroxybutyrate)	$P \propto r^n$, $n = 1.5$; 14.2	49
Poly(ethylene terephthalate)	$P \propto (\Delta T)^{-1.6}$	50
Ethylene carbonate with admixture of poly(acrylonitrile)	$P \propto (\Delta T - \Delta T_0)^{-1.1}$	51
Polyethylenes	$P \propto (\Delta T)^{-n}$, $n = 3.55-4.35$	52
Poly(D-lactide); Poly(L-lactide)	$P \propto (\Delta T)^{-7.2}$; $P \approx (\Delta T)^{-4.7}$	42b
Poly(3-hydroxybutyrate-co-3-hydroxyhexanoate)	$P \propto (\Delta T)^{-2.2}$	9
Maleic anhydride with admixture of poly(acrylonitrile)	$P \propto (\Delta T - \Delta T_0)^{-1.1}$	53
Poly(L-lactic acid) with additives	$P \propto (\Delta T)^{-n}$, $n = 2.3-8.1$	54
Isolated crystals		
Quartz	$P \propto r^{0.6}$	64c
Oxalic acid	$P \propto r^{0.3}$	64c
Hippuric acid	$P \propto r^{1.32}$	19

[a] More complicated behavior can take place.[64c] [b] Exponent is negative where data is plotted as function of ΔT.

Twisting Mechanism

Review of the Literature. By what mechanism do the crystals twist? This question has been reviewed in connection with optical banded spherulites of high molecular weight polymers

(47) Shuvalov, L. *Modern Crystallography, Vol. 4*; Springer: Berlin, 2005.
(48) Hobbs, J. K.; Binger, D. R.; Keller, A.; Barham, P. J. *J. Polymer Sci., Part B: Polym. Phys.* **2000**, *38*, 1575–1583.
(49) Barham, P. J. *J. Mater. Sci.* **1984**, *19*, 2781–2794.
(50) Keller, A. *J. Polym. Sci.* **1955**, *17*, 291–308.
(51) Sadlik, B.; Talon, L.; Kawka, S.; Woods, R.; Bechhoefer, J. *Phys. Rev. E* **2005**, *71*, 061602.
(52) Keith, H. D.; Padden, F. *J. Macromolecules* **1996**, *29*, 7776–7786.
(53) Degen, M. M.; Costanzino, N.; Bechhoefer, J. *J. Cryst. Growth* **2000**, *209*, 953–962.
(54) Xu, J.; Guo, B.-H.; Zhou, J.-J.; Li, L.; Wu, J.; Kowalczuk, M. *Polymer* **2005**, *46*, 9176–9185.

and minerals.[12a,52,55−58] Three mechanisms were proposed to explain twisting of polymer fibers. A fourth mechanism was applied to twisting of large single crystals. We discuss each of these in the context of HA.

(1) Axial Screw Dislocations in Thin Rods (Eshelby Twisting).[59] A screw dislocation with a Burgers vector parallel to the fiber axis forms a stress field that induces a twist moment in the fiber. Although this mechanism was found to operate in some special cases such as PbS[60] and PbSe[61] nanowires, it is unlikely to be applicable here. According to the Eshelby's mechanism, the twist period $P \approx 2\pi^2 r^2/b_v$, where r is the needle radius and b_v is the Burgers vector magnitude. For the [100] growth direction, the elementary Burgers vector $b_v = a/2 = 4.6$ Å. The typical needle is as thick as $2r \approx 5$ μm, predicting $P = 27$ cm, much longer than 1−4 mm observed. One can imagine axial dislocations with much larger Burgers vectors, but such giant dislocations are energetically unfavorable ($U \propto b_v^2$) and they should split (at least partially) into dislocations with smaller Burgers vectors.

(2) Fields. During crystallization, materials create thermal fields (from the latent heat of crystallization), mechanical fields (from density variation between crystal and melt), and compositional fields (from the concentration in the melt of impurities by the growing crystal). Such fields can lead to morphological instability and twisting.[57] HA fibers in spherulites have comparable twist periods and growth rates at very different temperatures (e.g., 70 vs 146 °C).[16−19] Viscosities and heat/mass transport should vary markedly at these temperatures. The twisting period in HA is comparable in individual needles and in spherulites of closely packed needles that form nearly planar growth fronts.[18] In banded HA spherulites, twist P varies with the crystallographic growth direction, thus arguing against mechanical and thermal fields.[18]

(3) Surface Stress. The outer layer of material always differs from the bulk due to the presence of noncompensated bonds giving rise to surface tension. Twisting requires differential stresses on the sides of a fiber. Specific etiologies for surface stress have been identified ranging from simple uniform stress due to differences in lattice constants between surface and bulk layers to impurity-mediated differences and varying tilts of polymer chains.[12] This latter mechanism is more likely to operate in polymer crystals because chain folding can accommodate significant elastic energy. On the contrary, HA is a typical small molecule crystal with a presumably thin and slightly distorted surface layer.[62,63] As we show below, a huge difference in volumes of the thin surface layer and crystal interior should prevent significant twisting even for high values of surface stress.

(4) Internal Stress. Absent from a discussion of high molecular weight polymer helical growth is heterometry stress, stress from within the crystal rather than from the outside. Low-symmetry crystals must be bounded by symmetry independent forms. Differences in structure and growth rates of symmetry independent facets in the presence of impurities can lead to differences in lattice constants in adjacent growth sectors, and ultimately to misfit (heterometry) stress and strain.[64] The stress distribution is controlled by the crystal morphology and under suitable conditions can provide a twist moment at the growth front leading to a macroscopic helix. This mechanism was originally proposed for twisting and bending of bulk crystals such as quartz, mica, oxalic acid, and gypsum.[64c,e,f] A similar idea (radial variation of Al impurity concentration) was used to explain fiber twisting in agates.[65,66] Impurities were also implicated in the twisting and bending of large dolomite crystals.[67]

Heterometry. Heterometry-induced crystal twisting requires compositional differences in the sectors comprising the needle tip. Observations show that the needle cross section is faceted. Ideally, the cross section is bounded by {011} faces and has a rhombic form with an acute angle of 80.0°. Morphologically such a section has two mirror planes along rhombus diagonals. This shape is inconsistent with formation of a twist moment, but crystallographically, the symmetry of HA is 222 (D_2), a point group wholly consistent with the development of a twist moment. Moreover, HA has a strong elastic anisotropy.[68] These features are consistent with the heterometry stress as the etiology of twisting.

For example, two possible scenarios for the generation of the twist moment are illustrated in Figure 11. We stress that these hypotheses cannot be evaluated in the absence of morphological characterization of the needle tips. This has not yet been achieved by electron microscopy. In Figure 11 we illustrate tip morphologies based upon the observed facets of single crystals. In the absence of mirror symmetry bisecting the tapered needled ends, (011) and $(0\bar{1}1)$ as well as $(01\bar{1})$ and $(0\bar{1}\bar{1})$ are not related by symmetry. These faces (marked gray and colorless, respectively) can differentially capture impurities and induce lattice misfit between corresponding {011} and {101} (light gray in Figure 11) growth sectors that results in a twist moment in the (100) plane. In a similar way crystallographic nonequivalence of {011} faces in the (100) plane can result in differential impurity incorporation along {011} faces (shown by graded coloration in Figure 11) that also can induce a twist moment in the (100) plane.

We can discriminate among the various proposals for twisting by estimating the elastic energy imparted by various causes. The elastic energy of the crystal, approximated as a twisted cylinder with a volume, $V = \pi r^2 l$, and a shear modulus, G, of ~5 GPa,[68] is equal to

(55) Sadlik, B.; Talon, L.; Kawka, S.; Woods, R.; Bechhoefer, J. *Phys. Rev. E* **2005**, *71*, 061602.
(56) Comer, J.; Ortoleva, P. *Am. Mineral.* **2007**, *92*, 1952–1957.
(57) Schultz, J. M. *Polymer* **2003**, *44*, 433–441.
(58) Keith, H. D.; Padden, F. J. *J. Polymer* **1986**, *27*, 1463–1471.
(59) Eshelby, J. D. *J. Appl. Phys.* **1953**, *24*, 176–179.
(60) Bierman, M. J.; Lau, Y. K. A.; Kvit, A. V.; Schmitt, A. L.; Jin, S. *Science* **2008**, *320*, 1060–1063.
(61) Zhu, J.; Peng, H.; Marshall, A. F.; Barnett, D. M.; Nix, W. D.; Cui, Y. *Nat. Nanotechnol.* **2008**, *3*, 477–481.
(62) De Vries, S. A.; Goedtkindt, P.; Huisman, W. J.; Zwanenburg, M. J.; Feldenhans, L. R.; Bennett, S. L.; Smilgies, D. M.; Stierle, A.; De Yoreo, J. J.; van Enckevort, W. J. P. *J. Cryst. Growth* **1999**, *205*, 202–214.
(63) Reedijk, M. F.; Arsic, J.; Kaminski, D.; van Enckevort, W. J. P.; Vlieg, E. *Surf. Sci.* **2003**, *526*, 133–140.
(64) (a) Chernov, A. A. *Modern Crystallography, Vol. 3*; Springer: Berlin, 1984. (b) Shtukenberg, A. G.; Punin, Yu. O. *Optically Anomalous Crystals*; Kahr, B., Ed.; Springer: Dordrecht, 2007. (c) Punin, Yu. O.; Shtukenberg, A. G. *Autodeformation Defects in Crystals*; St. Petersburg Univ. Press: St. Petersburg, 2008 (in Russian). (d) Shtukenberg, A. G.; Punin, Yu. O.; Artamonova, O. I. *Mineral. Mag.* **2009**, *73*, 385–398. (e) Moshkin, S. V.; Kuz'mina, M. A., Punin, Yu. O. *Physica Krislattizatsii*; Tver Univ. Press: Tver, 1991; pp 24−35 (in Russian). (f) Punin, Yu. O.; Artamonova, O. I. *Cryst. Rep.* **2001**, *46*, 138–143.
(65) Wang, Y.; Merino, E. *Am. J. Sci.* **1995**, *295*, 49–77. Wang, Y.; Merino, E. *Geochim. Cosmochim. Acta* **1990**, *54*, 1627–1638.
(66) Comer, J.; Oroleva, P. *Am. Mineral.* **2007**, *92*, 1952–1957.
(67) Radke, B. M.; Mathis, R. L. *J. Sed. Petrol.* **1980**, *50*, 1149–1168.
(68) Alex, A. V.; Philip, J. *Pramana-J. Phys* **2004**, *62*, 87–94.
(69) Bassett, D. C. *Principles of Polymer Morphology*; Cambridge Univ. Press: Cambridge, U.K., 1981.

$$U = \frac{\pi\theta^2 Gr^4 l}{4} = \frac{\theta^2 Gr^2 V}{4} \quad (6)$$

Although, we do not know the actual stress distribution within an HA needle, elastic energy can be roughly estimated using a bimetallic strip of the same volume. Individual layers are assumed to have thicknesses (h_1 and h_2) proportional to needle volumes of different compositions. At the boundary between layers, elastic strain $\varepsilon = \Delta a/a$ (a is a lattice constant) arises. In this case elastic energy of the strip is

$$U = \frac{\varepsilon^2 EV}{2} \cdot \frac{h_1 h_2}{(h_1 + h_2)^2} \quad (7)$$

If the elastic energy were the result of *surface stress* with a disrupted surface layer of approximately one unit cell, $\Delta r \approx$ 10 Å, and a Young's modulus of $E = 9$ GPa for HA,[68] the elastic energy can now be expressed through eq 7 as $U = \varepsilon^2 EV\Delta r/r$. Using the approximate experimental elastic energy from eq 6, we calculate $\varepsilon = 7.4\%$. This is an unrealistically large strain for a molecular crystal.[64c,69]

For *heterometry stress* the strain arises from a difference in lattice constants between growth sectors comprising the needle tip. If the sizes of these sectors are comparable, $h_1 = h_2$, the elastic energy from eq 7 can be estimated as $U = \varepsilon^2 EV/8$. This leads to a heterometry stress of $\varepsilon = 0.4\%$, which, though high, is conceivable. Expectations of growth sector specific differences in lattice constants can be judged from cinannamide, comparable in size to HA, solid solutions containing thienyl acrylamide.[70] Angular strain in the cinannamide system rises to 0.3%. Thus, an analysis of the elastic energies and strains induced by a variety of proposed etiologies for helical crystal twisting leads to the conclusion that heterometry stress is the most likely cause of twisting in HA. This conclusion may be applicable to other systems that have been observed to twist helically including high molecular weight polymers, minerals, elements, and other molecular crystals.[17]

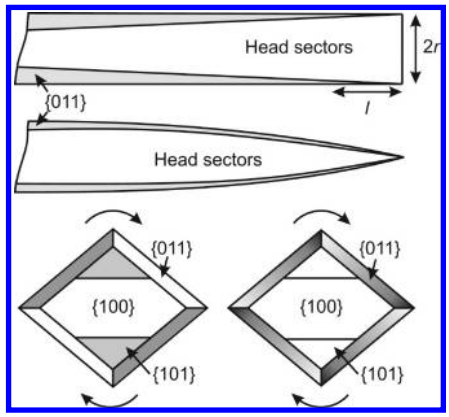

Figure 11. Idealized morphology of an HA [100] elongated needle-like crystal. Rectangular and wedge-like shapes of the crystal tip correspond to low and high supercooling and/or impurity concentrations, respectively. Graded coloration of {011} growth sectors in views of tip in bottom of the figure is aimed to show the possible inhomogeneity in impurity distribution along the face and the absence of mirror planes.

Conclusion

Helical growth morphologies of "single crystals" can be dynamic. Elastic stresses induced on different faces during growth of thin crystals can both twist and subsequently untwist fibers.

We have observed and surmised the following:

- Twisting is a two-stage process. Twisting at a needle growth front is followed by untwisting during crystal growth elsewhere.
- Both stages are ultimately plastic, not elastic.
- Untwisting stage can dramatically affect the twist period and provide a variety of morphologies within an ensemble.
- In the course of HA untwisting $P \propto h$.
- Sharpened needles, a consequence of impurity poisoning, result in stronger twisting.
- HA twisting is inconsistent with any previously articulated twist mechanisms except heterometry stress.

Acknowledgment. B.K. is grateful to the National Science Foundation for support through CHE-0349882. We also thank the donors of the Petroleum Research Fund of the American Chemical Society. Our appreciation is extended to S. Bian for assistance and E. Gunn for preliminary investigations.

Supporting Information Available: SM1: A movie of an HA crystal twisting during growth. This material is available free of charge via the Internet at http://pubs.acs.org.

JA101491N

(70) Vaida, M.; Shimon, L. J. W.; Weisinger-Lewin, Y.; Frolow, F.; Lahav, M.; Leiserowitz, L.; McMullan, R. K. *Science* **1988**, *241*, 1475–1479.